Berichte aus dem Zentrum für Meeres- und Klimaforschung
Reihe A: Meteorologie

Nr. 11

ARKTIS 1993

Report on the Field Phase with Examples of Measurements

Edited by

Burghard Brümmer

Meteorologisches Institut
Hamburg 1993

2.3. *Ice floe station*

(G. Peters[1], M. Claussen[2], H. Lohse[3], A. Grelle[4], L. Kornblüh[3], B. Fischer [1]

1: Meteorologisches Institut der Universität Hamburg
2: Max-Planck-Institut für Meteorologie, Hamburg
3: GKSS Forschungszentrum, Geesthacht
4: Swedish University of Agricultural Sciences, Uppsala)

2.3.1 *Overview*

The ice floe station was installed in the immediate vicinity of POLARSTERN at 81° 28' N, 07° 37' E in about 60 miles distance from the ice margin. The ship was moored on 8 March to a large ice-field at the north-east side of an initially open lead. Only on this side of the lead the ice was solid enough to carry heavy equipment. Nevertheless, it turned out that only small portable instruments could be deployed on the ice because the hatches of the ship were sealed by a heavy ice cover and because the cranes did not work due to low temperatures. For the same reason the containers with power supplies and data recording units had to remain on the ship. Therefore not all instruments could be positioned as far from the ship as desirable for undisturbed measurements. The locations of all measuring systems relative to the ship and the lead are shown in Figure 2.3.1.

The measurements did not start before 11 March because the low temperatures which prevailed during the first days made the installation work very difficult. As far as wind, air temperature and humidity measurements are concerned the ship's disturbance was acceptably small because the sensors were never in lee of the ship. On the other hand the radiation sensors were sometimes in the ship's shadow. Fortunately redundant sensors could be installed at different sites giving the possibility to identify shadow effects.

Most of the instruments were aligned on a NW-SE-axis close to the straight rim of the ice floe which had been shaped by the ship prior to the instruments' installation. One Sonic anemometer (position 1a) was mounted on a boom over the lead in order to get the sensible heat flux over the thin ice. The surface structure around the measuring site is indicated in Figure 2.3.1. In the NW corner ridges higher than 2 m were the most pronounced structures. All other ridges were less than 1 m high. By the shaping of the rim a field of ice debris was produced in the lead which is also indicated in the figure.

The surface structure in the farther environment of the ice floe station was surveyed by altimeter measurements with a helicopter. The flight pattern and the surface structure of the farther environment on 18 March is shown in Figure 2.3.2.

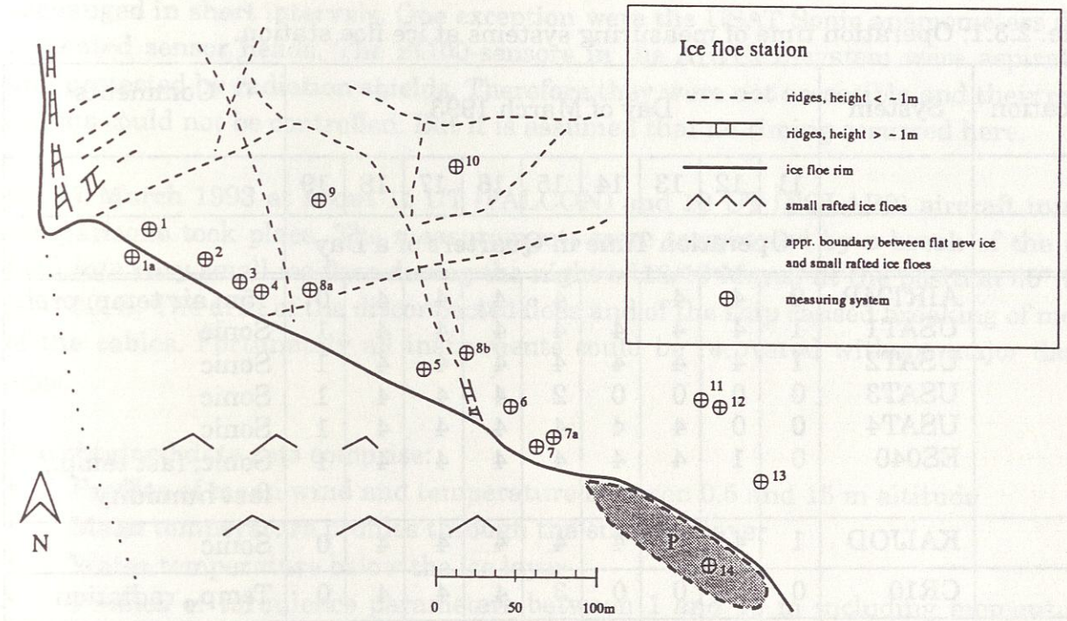

Figure 2.3.1: Locations of measuring systems at ice floe stations. For explanation of numbers see Table 2.3.1.

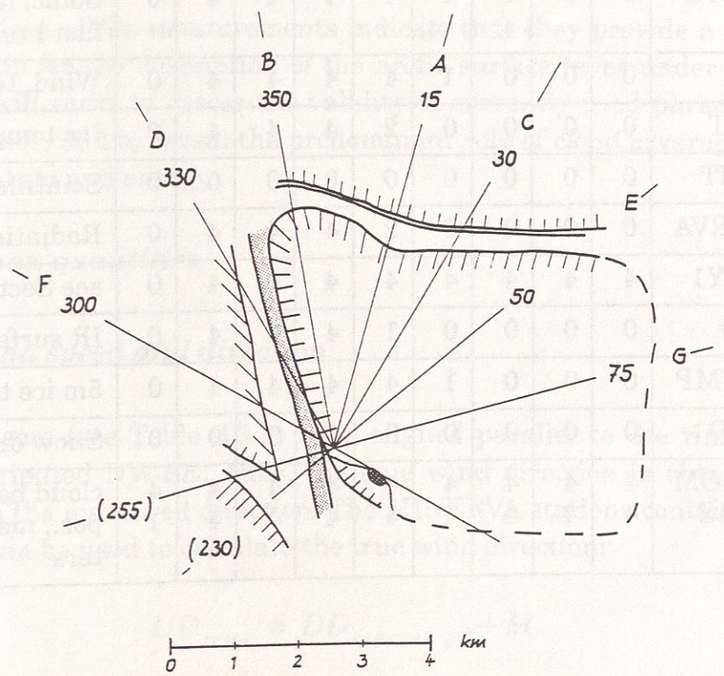

Figure 2.3.2: Helicopter flight pattern and farther environment of the ice station on 18 March. The numbers indicate the flight leg azimuths in degrees. The capital letters A to G show the temporal order of flights.

Table. 2.3.1: Operation time of measuring systems at ice floe station.

Location	System	Day of March 1993									Comments
		11	12	13	14	15	16	17	18	19	
		Operation Time in Quarters of a Day									
1	AIRTMP	2	4	4		4	4	4	4	0	15m air temp. prof.
	USAT1	1	4	4	4	4	4	4	4	1	Sonic
	USAT2	1	4	4	4	4	4	4	4	1	Sonic
	USAT3	0	0	0	0	2	4	4	4	1	Sonic
	USAT4	0	0	4	4	4	4	4	4	1	Sonic
	ES040	0	1	4	4	4	4	4	4	1	Sonic; fast temp., fast humidity
1a	KAIJOD	1	4	4	4	4	4	4	4	0	Sonic
2	CR10	0	0	0	0	3	4	4	4	0	Temp., radiation
3	BUOY2	0	0	0	0	2	4	4	4	0	see Section 2.4
4	MINRVA	2	4	4	4	4	4	4	4	0	Temp.
5	SOLENT	2	4	4	4	4	4	4	4	0	Fast temp., fast humidity, fast CO_2
6	ES010G	0	3	4	4	4	4	4	4	0	Sonic; fast temp., fast humidity
7	CR7	0	0	0	1	4	4	4	4	0	Wind, temp., rad.
7a	BODT	0	0	0	0	2	4	4	4	0	Ice temp.
8, 8a	SCINT	0	0	0	0	0	0	0	0	0	Scintillometer
9	MINRVA	0	0	0	0	2	4	4	4	0	Radiation
10	BUOY1	4	4	4	4	4	4	4	4	0	see Section 2.4
11	KT19	0	0	0	0	1	4	4	4	0	IR surface temp.
12	ICETMP	0	0	0	1	4	4	4	4	0	5m ice temp. prof.
13	SNOD	0	0	0	0	0	0	0	0	0	Snow drift
14 14	CEILOM INDAS	4 4	4 4	4 4	4 4	4 4	4 4	4 4	4 4	4 1	cloud base pos., met. parameters

All air sensors were subject to considerable riming and had to be cleaned or exchanged in short intervals. One exception were the USAT Sonic anemometers due to heated sensor heads. The Pt100-sensors in the AIRTMP-system were aspirated and protected by radiation shields. Therefore they were not accessible and their conditions could not be controlled. But it is assumed that no riming occurred here.

On 17 March 1993 at about 11 UT (FALCON) and 13 UT (POLAR2) aircraft intercomparisons took place. The measurements were terminated by a break of the ice field into very small ice floes during the night of 18/19 March at the position 80° 29' N 4° 02' E. The drift of the disconnected floes and of the ship caused breaking of most of the cables. Fortunately all instruments could be recovered without major damages.

The obtained data sets comprise:

- Profiles of mean wind and temperature between 0.5 and 15 m altitude
- Mean temperature profiles through the snow/ice layer
- Water temperature below the ice layer
- Profiles of turbulence parameters between 1 and 15 m including momentum flux and sensible heat flux
- Latent heat flux
- Up- and downwelling short- and longwave radiation
- Snow surface brightness temperature
- Cloud base altitude

First inspections of the measurements indicate that they provide a short but fairly complete basis for the description of the arctic surface layer under winterly conditions. They will serve to assess the validity of currently used parameterizations of turbulent fluxes, and to reveal the predominant role of cloud coverage on the budgets of momentum and energy.

2.3.2 Mean quantities

a. Wind speed and direction

All wind sensors (see Table 2.3.2) were aligned parallel to the rim of the ice floe which was oriented NW-SE. Thus, the true wind direction is obtained by adding about 315° to the measured direction. The MINERVA stations contained magnetometers which can be used to calculate the true wind direction:

$$DD_{true} = DD_{measured} + M \qquad (1)$$

The pathname of the magnetometer azimuth data M is: arktis.IX.1a/minerva.z./KW.

This correction has already been done on-line for the minerva wind measurements.

USAT1 was misaligned by about 15°. The exact value has still to be determined from the continuity of measured direction profiles and from photographs.

Table 2.3.2: Sensors measuring wind speed and direction at ice floe station.

Location No.	Height [m]	System	Name of Parameter	Remarks
1a	01.45	KAIJOD	vel, dir	Kaijo-Denki Sonic mounted on a boom over the lead
1	03.65	ES0400	U, DD	Kaijo-Denki Sonic mounted on 2 m NW-pointing boom at 15 m mast 1 m SW of USAT4
1	03.65	USAT4	vel, dir	METEK Sonic mounted on 2 m NW-pointing boom at 15 m mast 1 m NE of ES0400
1	07.10	USAT3	vel, dir	METEK Sonic mounted on 2 m NW-pointing boom at 15 m mast
1	10.00	USAT2	vel	METEK Sonic mounted on 2 m NW-pointing boom at 15 m mast
1	15.10	USAT1	vel, dir	METEK Sonic on top of 15 m mast
3	02.00	BUOY2		See Section 2.4
4	02.00	MINRVA	FFr DDr FFBr FFa DDa FFBa	cup anemometer (MPI) wind vane (MPI) relative wind speed magnitude true wind speed true wind direction true wind speed magnitude only 1 day useful data
5	03.00	SOLENT	vel, dir	SOLENT ultraSonic anemometer mounted on top of a pole
6	04.15	ES010G	U	Kaijo-Denki Sonic
7	04.03	CR7	WGS DU	cup anemometer (type 999) wind vane
10	02.00	BUOY1		See Section 2.4
14	37.00	INDAS	vel, dir	true wind speed and direction

b. Air temperature

All air temperature sensors are listed in Table 2.3.3. The sensors at the 15 m mast (location 1, AIRTMP) need to be recalibrated. Preliminary evaluations show offsets up to 1.0 K but there is no indication of significant drift of calibration. The mean virtual temperatures measured by the ultra Sonic anemometers have also been archived. Contamination of the sensors and mechanical distortions of the mounting structure may cause offsets up to some K. Therefore these measurements should be used cautiously.

Table 2.3.3: Sensors measuring air temperatures at ice floe station.

Location No.	Height [m]	System	Name of Parameter	Remarks
1	00.92	AIRTMP	0.92 m	sensor id.: 101
	01.86		1.86 m	sensor id.: 309
	02.98		2.98 m	sensor id.: 308
	03.90		3.90 m	sensor id.: 307
	04.89		4.89 m	sensor id.: 106
	06.00		6.00 m	sensor id.: 305
	06.71		6.71 m	sensor id.: 304
	07.92		7.92 m	sensor id.: 303
	09.92		9.92 m	sensor id.: 302
	14.70		14.70 m	sensor id.: 301
	03.40	ES0400	TD	dry temperature (no valid data)
	03.40	ES0400	TW	wet bulb temp. (no valid data)
	03.40	ES0400	T3	temperature
	03.65	USAT4	T	virtual temperature
	03.65	ES0400	TV	virtual temperature
	07.10	USAT3	T	virtual temperature
	10.00	USAT2	T	virtual temperature
	15.10	USAT1	T	virtual temperature
1a	01.45	KAIJOD	T	virtual temperature
2	01.52	CR10	TL	METEK Sonic mounted on 2 m NW-pointing boom at 15 m mast 1 m NE of ES0400
3	02.00	BUOY2		see Section 2.4
4	01.40	MINRVA	BPTT	Air temperature (Friedrichs)
	00.50		TT	Air temperature dew point minor
5	03.00	SOLENT	A1	fast temperature
			T	virtual temperature
6	03.90	ES010G	TD	dry temperature (no valid data)
			TW	wet bulb temp. (no valid data)
			T3	temperature
	04.15		TV	virtual temperature

Table 2.3.3: Sensors measuring air temperatures at ice floe station.

Location No.	Height [m]	System	Name of Parameter	Remarks
7	04.03	CR7	TL	temperature
10	02.00	BUOY1		see Section 2.4
14	27.00	INDAS	airtemp	temperature

c. Mean temperature profiles in snow, ice and water

All sensors measuring the snow, ice or water temperature are listed in Table 2.3.4. Snow and ice temperature profiles have been measured at two sites (7a and 12). Due to problems with the ice drills, the start of the measurements was delayed by some days. The temperature disturbance within the ice which was caused by the drilling and by the temporary removal of the snow cover was significant for another couple of days. Consequently the solid ice temperatures are representative only during the last two measuring days.

At location 12 the lower 5 measuring depths were below the ice and show the water temperature. The ice core has been preserved and is archived under reference no. R9107302 at the Alfred-Wegener-Institut in Bremerhaven. Above the solid ice there are two sets of measurements:

a. The sensors at 0.0, 0.3 m, 0.6 m, 0.9 m were mounted in the upper part of the rod used for the ice profile. The snow cover was about 40 cm. So 0.6 m and 0.9 m represent air temperatures. The sensors had no radiation shield and they were not aspirated, so that the corresponding values are subject to radiation errors. The measurement at 0.3 m is also of questionable value as the snow cover was artificially prepared here and not in its original condition.

b. The sensors at 0.00 m, 0.09 m, 0.18 m, 0.26 m, 0.34 m, 0.42 m are glass covered Pt100-sensors which were positioned into the undisturbed snow cover without any artificial mounting structure. In order to put them into defined positions a vertical cross-section was digged cautiously down to the solid (very plain) ice surface. Then holes of 6 mm diameter and of 50 cm length were drilled horizontally into the snow through the vertical surface at the desired altitudes, and the sensors were pushed into the holes using stiff white-coated connection wires. The horizontal distance of the sensors from the rod was 1.2 m. Finally the ditch was refilled with snow in order to reduce the disturbance.

Six profiles of snow density and crystal structure have been taken in 50 cm distance from the temperature profile position (Evaluation: Bettina Loth, MPI, and Eileen

Aldsworth, SPRI). Qualitatively, a lower layer of coarse-grained-high-density and an higher layer of fine-grained-low-density could be distinguished. The interface between these layers was at an altitude of 18 ± 2 cm above the ice surface.

Table 2.3.4: Sensors measuring snow, ice or water temperature

Location No.	Height [cm]	System	Name of Parameter	Remarks
2	Mean from 0 to -8 Mean from 0 to -8	CR10	TB0 TB2	Height relative to snow surface on 15 March 1993
7	Mean from 0 to -8 -0.02 -0.05 999	CR7	TB01 T2 T1 T3	Height relative to snow surface on 15 March 1993. Data not useful.
7a	0.05 m steps from -0.28 m up to 0.18 m	BODT	-0.28m 0.18m	Height relative to ice surface.
12	0.3 m steps from -3.00 m to 0.90 m	ICETMP	-3.0m. . . . 0.9m	Height relative to ice surface. rod mounted rod mounted
12	8 cm steps from 0.0 m up to 0.42 m		0.00m 0.42m	Height relative to ice surface. Single sensors without disturbing mounting struct.

2.3.3. Turbulence: variances and covariances

The turbulent fluctuations of wind components and virtual temperature have been measured with different types of Sonic anemometers. In addition the temperature and humidity have been measured at some locations with high temporal resolution synchronously with the Sonic measurements. All covariances with the vertical wind component and a selected set of further covariances and turbulence parameters have been calculated online every 5 minutes. For short intervals raw data have been recorded with high temporal resolution. Details of the coordinate transformations, tilt corrections etc. are described in the Sonic operating manual (USAT-3 Bedienungshandbuch, METEK GmbH, Hamburg, 1990). Three types of sonics (KAIJO DENKI TR61, USAT-3, and SOLENT) and two types of fast humidity sensors (Campbell Lyman alpha and LI-COR LI6262) have been used. The LI-6262 is a gas analyzer, which provided H_2O- and, in addition, CO_2-concentrations with 10 Hz sampling rate.

Table 2.3.5: Instruments measuring turbulence parameters.

Location No.	Height [cm]	System	Name of Parameter	Remarks
1	03.65 03.40 03.40 03.65 07.10 10.00 15.10	ES400 USAT4 USAT3 USAT2 USAT1	see Appendix G see Appendix G see Appendix G see Appendix G see Appendix G	Sonic Fast temperature Lyman-alpha Temporarily only mean values useful
1a	01.45	KAIJOD	see Appendix G	Relative to thin ice surface
5	03.00	SOLENT	see Appendix G	Sonic, fast temperature, fast humidity, fast CO_2
6	04.15 03.90 03.90	ES010G	see Appendix G	Sonic Fast temperature Lyman-alpha

2.3.4. *Radiation fluxes*

Auxiliary parameters as body and calotte temperatures of the radiation sensors are not mentioned here but are documented in Appendix G. The following abbreviations are used in Table 2.3.6: S = shortwave radiation; L = longwave radiation; ↑ = upwelling; ↓ = downwelling.

Table 2.3.6: Instruments measuring radiation parameters.

Location	System	Name of Parameter	Remarks
2	CR10	GSK1	Photosynthetically active radiation 400-700 nm [µMol s/m^2]
		GS	Global radiation
		STB	S↑ + S↓ + L↑ + L↓ [W/m^2]
		STBO	S↓ + L↓ [W/m^2]
		STBU	S↑ + L↑ [W/m^2]
		STB1	S↑ + S↓ + L↑ + L↓ [W/m^2]
		STB1O	S↓ + L↓ [W/m^2]
		STB1U	S↑ + L↑ [W/m^2]

Table 2.3.6: Instruments measuring radiation parameters.

Location	System	Name of Parameter	Remarks
7	CR7	GSK1	Photosynthetically active radiation 400-700 nm [µMol s/m^2]
		GSK2	Data not useful
		GSK3	Data not useful
		GS	Global radiation [W/m^2]
		STB	S↑ + S↓ + L↑ + L↓ [W/m^2]
		STB1	S↑ + S↓ + L↑ + L↓ [W/m^2]
		STB1O	S↓ + L↓ [W/m^2]
		STB1U	S↑ + L↑ [W/m^2]
9	MINRVA	GO	Kipp + Zonen pyranometer S↓ [W/m^2]
		Gu	Kipp + Zonen pyranometer S↑ [W/m^2]
		Iro	Eppley pyrgeometer L↓ [W/m^2]
		Iru	Eppley pyrgeometer L↑ [W/m^2]
		LWo	Eppley pyrgeometer L↓ [W/m^2]
		LWu	Eppley pyrgeometer L↑ [W/m^2]
		A	Schulze-Lange S↓ + L↓ [W/m^2]
		E	Schulze-Lange S↑ + L↑ [W/m^2]
		B	Schulze-Lange S↓ + L↓ + S↑ + L↑ [W/m^2]
11	KT19	TS	Brigthness temperature of snow surface
14	INDAS	radiat	Global radiation [W/m^2]

2.3.5. *Examples of measurements*

Figures 2.3.3 - 2.3.8 show data of some selected sensors on 16 March 1993. This 24 h interval has been chosen to demonstrate the predominant role of cloud cover on the energy budget and the dynamics of the surface layer.

In Figure 2.3.3 a time-height cross section of the ceilometer backscatter intensity is shown. The ground observations reported light snow fall or single ice cristals during the whole 24 h period. In addition, moist haze was observed during the daytime. This is probably the source of the spacially continuos echo structure which reaches down to the surface. The upper edge of the echo profiles shows a maximum most of the time before 21 UT. This is interpreted as the base of optically thick clouds. At 21 UT the backscatter echo vahishes completely, which is consistent with the observed low stratus and stratus fractus cloud cover and with the decrease from 8/8 to 1/8 coverage after 20 UT.

The ceilometer profiles can be related to the radiation budget R shown in Figure 2.3.4. The thick dashed line represents -R based on the data of MNRVA. In this convention a positive budget means an upward directed net flux. The most outstanding feature of this time series is the jump from small negative values to values higher than R = 40 W/m^2 at about 21 UT. This coincides with the vanishing upper edge of the ceilometer profile and the reported decrease of cloud coverage after 20 UT.

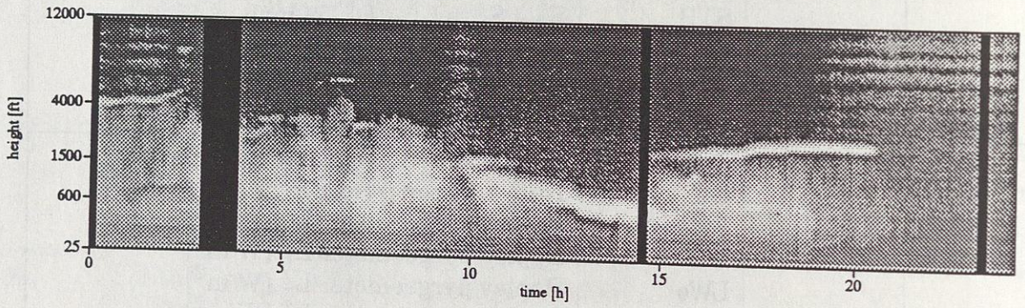

Figure 2.3.3: Ceilometer backscatter profiles.

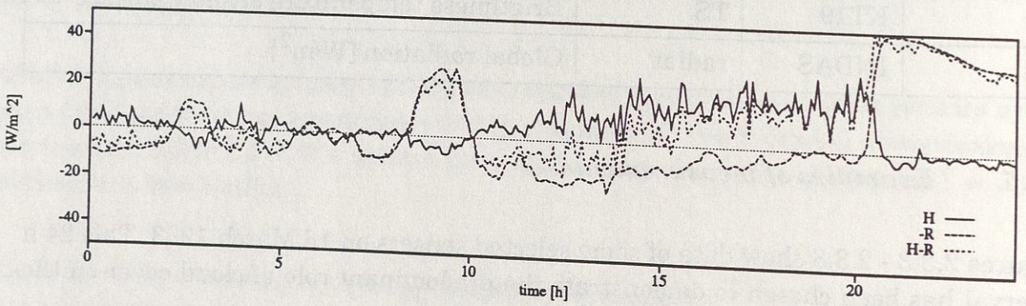

Figure 2.3.4: (Negative) radiation budget - R, sensible heat flux H, and sum of both.

Further inspection shows two more positive peaks of R around 03 and 09 UT. The major peak at 09 UT coincides with a minimum of the backscatter intensity (interuption of snow fall) and a cloud gap as mesaured by the ceilometer. The minor peak at 03 UT can hardly be related to special features in the ceilometer profiles. The snowfall seems to continue but the maximum at the upper edge of the profile (which we assume to indicate the cloud base) fades out at that time.

After the second maximum of R at about 10 UT a low cloud base appears in the ceilometer data. It starts at 1000 ft and sinks continuously down to 400 ft until 15

UT, when a higher cloud deck becomes visible. Probably the higher clouds exist already earlier but are not visible until the lowest layer disappears. This higher cloud layer remains at a fairly constant altitude of about 2000 ft until 21 UT.

The surface is obviously not in radiative equilibrium with the cloud base as the radiation budget R is negative (net downward flux) during most of the time interval between 10 and 21 UT. R approaches nearly zero at 19 UT and remains at little values for 2 h until the cloud cover disappears. If this temporal variation of R is fitted by an exponential function, the corresponding time constant would be about 5 h.

The general features of R are consistent with the radiosonde profiles which show a ground based inversion with its temperature maximum at about 1000 m. According to this the cloud base is expected to be up to 10 K warmer than the surface. R is also negative in the earlier cloud covered intervals (00 - 02 UT and 04 - 08 UT) but the absolute values are smaller here. It is assumed that the stronger precipitation and haze before 08 UT (which made the cloud base sometimes invisible for the ceilometer) shifts the maximum of the contribution function for downwelling radiation to lower altitudes with lower temperatures.

In Figure 2.3.4 also the sensible heat flux H measured by the Sonic USAT1 at 15.1 m altitude is shown. The qualitative features of this time series appear to be plausible as H is anticorrelated to the radiation budget. Only the sign of the soil energy flux as calculated by the residual Q_s = H - R (thin dashed line) raises some questions. Between 10 and 14 UT Q_s is directed downward which should cause an inversion of the soil temperature profile at least in the upper few centimeters below the surface. This does not occur, as to be seen in Figure 2.3.5, which shows 30 min averages of water/ice/snow temperature profiles. The temperature gradient is always negative even in the highest 6 cm below the surface, although it is less steep during the cloud covered periods.

Several possible explanations for this discrepancy have to be considered in a more careful analysis. The most likely reasons are:

a. R may have an offset of a few W/m^2. This can be checked, as there is ample redundancy of radiation measurements.
b. The turbulent heat flux at 15 m may not represent the surface flux, but some flux divergence may to be taken into account in the intermediate layer. This can also be checked using lower altitude flux data.
c. The heat flux as derived by Sonic is underestimated. This error is rather unlikely because first side by side intercomparisons with heat fluxes derived by independent fast temperature measurements indicate a deviation (if at all) into the opposite direction (not shown here).
d. In this discussion the latent heat flux has not been included as this quantity is

of questionable significance due to the small measured values. According to measurements of two independent systems the latent heat flux varies between ± 2 W/m^2. If this order of magnitude is correct it does not explain the discrepancy.

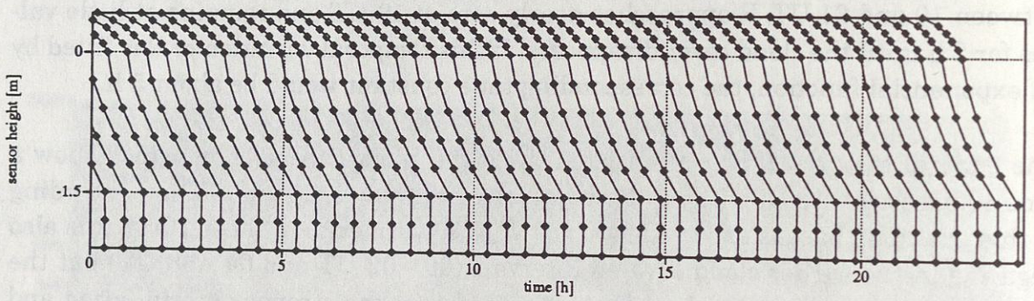

Figure 2.3.5: Profiles of water, snow and ice temperature (30 min averages). Subsequent profiles are shifted by 5 K. Ice-snow interface at 0 m, ice-water interface at -1.5 m.

Figure 2.3.6 shows the inverse Monin-Obukhov length derived from the USAT1 flux measurements. It is correlated with R in the expected way.

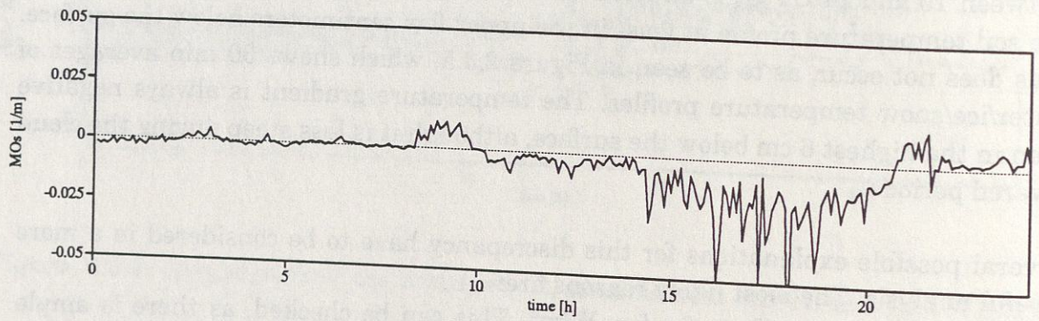

Figure 2.3.6: Inverse Monin-Obukhov length 1/L.

The temperature time series in Figure 2.3.7 are based on measurements at 1.4 m by Pt100 sensor MNVRA/BPTT and at 15.1 m by Sonic USAT1/T. These different sensors have been selected here in order to demonstrate two things:

a. The Sonic temperatures, although sensitive to sensor contaminations, seem to reproduce the overall variation quite realistically. Thus, these data are reproduce the overall variation quite realistically. Thus, these data are probably useful to support the analysis of the other temperature measurements. In contrast to measurements with conventional contact sensors the Sonic temperatures are not affected by radiation errors, riming (thanks to heating of the sound transducers), or by variable ventilation effects.

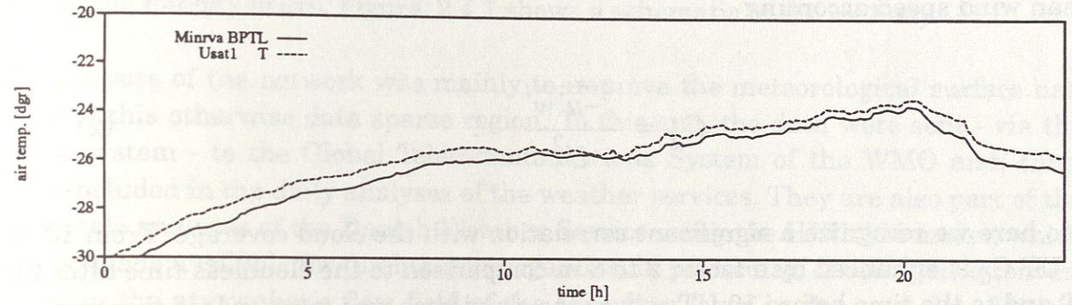

Figure 2.3.7: Temperature measured at 1.4 m by a Pt100 sensor and at 15.1 m by a Sonic.

b. The variablity of the temperature difference between 1.4 m and 15.1 m is also consistent with the radiation budget and the sensible heat flux. The stability of the stratification is smaller during the time interval 10 - 20 UT with negative radiation budget and positive turbulent heat flux. Under stationary conditions one would expect even an unstable stratification which is not observed here. This may either be explained by advective effects (the general temperature trend until 20 UT indicates warm air advection) or by an offset of the Sonic temperature of about 0.5 K which would be well within the instruments specifications. The basic data which should be used to analyze the thermal atmospheric stratification are the 10 Pt100 temperatures measured at the 15 m mast (not shown here).

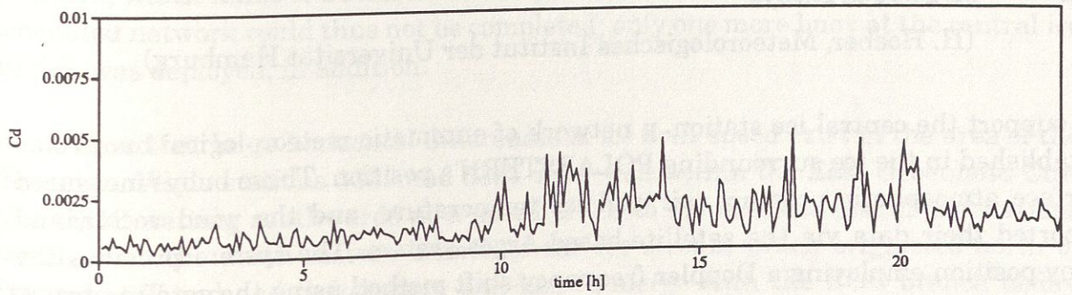

Figure 2.3.8: Drag coefficient measured at 15.1 m.

Figure 2.3.8 shows the drag coefficient as derived from the momentum flux and the mean wind speed according

$$C_d = \frac{\sqrt{-u'w'}}{U^2} \quad . \qquad (2)$$

Also here we recognize a significant correlation with the cloud coverage. From 10 to 21 UT C_d is enhanced by a factor 2 to 3 in comparison to the cloudless time after 21 UT and to the time before 10 UT, where the cloud base was more or less obscured by snow and haze.

Some preliminary conclusions can be derived already from this short data set. The ground based inversion, which is a general feature of the winterly arctic boundary layer, is responsible for the observed effects of cloud coverage: In cloudless conditions the energy exchange at the surface is dominated by radiative transfer. On the other hand, in case of cloud cover, a significant portion of the heat exchange between the snow/ice covered surface and the atmosphere may be carried by the turbulent sensible heat flux. Although the absolute values of the turbulent heat flux are not very big its effect on the surface drag is striking. The turbulent friction, which is generally very low in the stable surface layer, increases dramatically in case of cloud coverage (and absence of precipitation/haze).

The complete observations during this campaign provide a unique basis to quantify these effects, which seem to be characteristic for the winterly arctic ocean, and to include other effects as variable z_0 according to the ice surface structure and the possible dependence of turbulent friction on snow drift.

In addition, the ice temperature profiles, the high resolution snow temperature profiles in conjunction with the well documented ice and snow structure should be useful to improve the understanding of the soil heat budget including phase transitions.

2.4. *Argos Ice Buoys*

(H. Hoeber, Meteorologisches Institut der Universität Hamburg)

To support the central ice station, a network of automatic meteorological buoys was established in the ice surrounding POLARSTERN's position. These buoys measured surface atmospheric pressure, air and ice temperature, and the wind vector, and reported their data via the satellite-based Argos system. The system provides the buoy position employing a Doppler frequency shift method using the satellite transmission link. Sampling frequency of the stations was one per hour, and data is available, when a satellite was overhead to receive the transmission. With two satellites in orbit, this was the case at an average of more than one per hour between 16 UT in